

A network model to investigate structural and electrical properties of proteins

Eleonora Alfinito, Cecilia Pennetta, and Lino Reggiani

Dipartimento di Ingegneria dell'Innovazione, Università del Salento

Via Arnesano, I-73100, Lecce, Italy,

*Consorzio Nazionale Interuniversitario per le Scienze Fisiche della Materia (CNISM)**

(Dated: July 14, 2021)

Abstract

One of the main trend in to date research and development is the miniaturization of electronic devices. In this perspective, integrated nanodevices based on proteins or biomolecules are attracting a major interest. In fact, it has been shown that proteins like bacteriorhodopsin and azurin, manifest electrical properties which are promising for the development of active components in the field of molecular electronics. Here we focus on two relevant kinds of proteins: The bovine rhodopsin, prototype of GPCR protein, and the enzyme acetylcholinesterase (AChE), whose inhibition is one of the most qualified treatments of Alzheimer disease. Both these proteins exert their functioning starting with a conformational change of their native structure. Our guess is that such a change should be accompanied with a detectable variation of their electrical properties. To investigate this conjecture, we present an impedance network model of proteins, able to estimate the different electrical response associated with the different configurations. The model resolution of the electrical response is found able to monitor the structure and the conformational change of the given protein. In this respect, rhodopsin exhibits a better differential response than AChE. This result gives room to different interpretations of the degree of conformational change and in particular supports a recent hypothesis on the existence of a mixed state already in the native configuration of the protein.

*Corresponding author e-mail: eleonora.alfinito@unile.it

I. INTRODUCTION

Proteins are at the basis of living systems. In particular, they control the sensing action and the correct functioning of the system by operating at a cellular level. In a cell, the starting process of this functional control is usually associated with a conformational change of the protein in response to the capture of a specific ligand. The conformational change activates a sequence of biological mechanisms, which end in the production of a final stimulus used by the system to organize its life. The possibility to detect such a conformational change through some modification of an electrical property of the corresponding protein is of extreme interest from both a fundamental and an applied point of view.

On the former side, the nature of charge transport in protein [1] and, in general, in biological matter [2], is a long time explored subject till now not completely understood [3]. Most of the models are based on a quantum mechanical tunneling [3]. On this respect, some lean towards a charge transport along the protein backbone [4], others point to a "rest and fire" thermal mechanism in which charge is injected only for certain values of the dihedral angles [5].

On the latter side, applications, the use of proteins, and in general of biomolecules, for the construction of nanodevices is one of the leading frontiers in biology, physics and technology. In fact, there are various concomitant peculiarities which point to biomolecules as promising material for new devices. Among them, we remember their extremely small sizes, their specificity, i.e. the ability to react only to a specific stimulus (or a very narrow window of similar stimuli), their conductive properties [6, 7], and not negligible, their low cost [8].

In this context, the most intriguing problem is to understand how conformational changes influence the electrical properties of a protein. At present, most of the information about the different structures of proteins comes from X-ray or NMR investigations [9]. The polypeptide is crystallized (X-ray analysis) and then a map of all its atoms is acquired. Starting from these representations it is possible to model the protein by using, either an all-atom scheme like in Molecular Dynamics techniques [10], or an all-amino acid scheme like in Elastic Network models [11, 12, 13, 14]. The former method is surely more accurate but needs for a big computational environment, the latter method requires more affordable computational resources and anyway is able to catch the relevant features of the polypeptide. Many authors have described the topological and statistical properties of this kind of network, also inducing physical information in fine accordance with the experimental tests [11, 12, 13, 14].

The aim of this paper is to develop an irregular network model, which translates a given protein topology into the protein electrical properties. Accordingly, starting from the three-dimensional representation of the protein, the model will carry out a comparative analysis of its geometrical structures and predict some features of its small signal impedance. Calculations are specialized to bovine rhodopsin, the prototype of G-protein coupled receptors (GPCR), and to the enzyme AChE, whose inhibition is one of the most qualified treatments of Alzheimer disease. By means of Nyquist plots, the electrical response of the corresponding networks are then investigated for different values of frequency of the applied external field.

The content of the paper is organized as follows. Section II briefly reviews the theoretical approach. Section III reports the results obtained for the two proteins considered here by analyzing the topological network and the impedance spectra for the known structures available in the literature. Major conclusions are drawn in Sec. IV. Finally, the Appendix details the values of the protein equivalent circuit obtained from the simulations.

II. MODEL

Since the seminal paper of Tirion [12], many researchers have investigated the possibility to model proteins by means of appropriate networks [13, 14]. This coarse grained approach is computationally more affordable than a molecular dynamics procedure [10] and, nevertheless, able to simulate the global behavior of a given protein [12, 13, 14]. Within this approach, a protein is mapped into a network whose nodes coincide with the coordinates of the so-called C_α carbon atom pertaining to each amino acid as known from the public data base (PDB) [9]. As free parameter, the model contains the interaction (cut-off) radius, \mathbf{R} , which fixes the maximal distance between two connected nodes: Only nodes with distance less or equal to \mathbf{R} are connected with a link. This simple model provides a map of the protein spatial organization, i.e. a topological network or a graph. It becomes pregnant of meaning only when the links take a physical role. This was made, for example, by assigning a spring constant to each link and thus studying the network normal modes [12, 13, 14].

In some recent works [15, 16, 17], by assigning to each link an impedance, we proposed a new strategy for the investigation of the protein electrical response. Furthermore, on the same ground, also the role of thermal fluctuations was tested [15, 16, 17]. Here we use the same strategy by assuming that the amino acids interact electrically among them: The electrical charge transfers between neighboring residues [18], which can also change their electronic polarization [19]. More precisely, in this model each link between the nodes i and j corresponds to an elementary RC parallel impedance $Z_{i,j}$, with R an Ohmic resistor and C a planar homogeneous capacitor. By assuming that the cross-sectional area of resistor and capacitor is equal to the cross-section area of overlapping spheres, the elementary impedance becomes [16]

$$Z_{i,j} = \frac{l_{i,j}}{\mathcal{A}_{i,j}} \frac{1}{(\rho^{-1} + i\epsilon_{i,j} \epsilon_0 \omega)} \quad (1)$$

where $\mathcal{A}_{i,j} = \pi(\mathbf{R}^2 - l_{i,j}^2/4)$, is the cross-sectional area between the spheres centered on the i, j nodes, respectively, $l_{i,j}$ is the distance between these centers, ρ is the resistivity, taken to be the same for every amino acid with the indicative value of an insulator $\rho = 10^{10} \Omega \text{ m}$; i is the imaginary unit, $i = \sqrt{-1}$, ϵ_0 is the vacuum permittivity and ω is the circular frequency of the applied voltage. The relative dielectric constant of the couple of i, j amino acids, $\epsilon_{i,j}$, is expressed in terms of the intrinsic polarizability of the i, j amino acids, α_i, α_j [16, 19] as:

$$\epsilon_{i,j} = 1 + g \left[\frac{(\alpha_i + \alpha_j)}{2} - 1 \right] \quad (2)$$

where $g=4.65$ is a normalization constant introduced to obtain values of $\epsilon_{i,j}$ distributed between 1 and 80 (relative permittivity of vacuum and water at 20 °C, respectively).

By taking the first and last amino acid as injector and collector contacts at the given electrical potential difference, the calculation of the total impedance of the network is obtained by solving the electrical circuit, i.e. we have found the potential on each node and the current flowing through each link for a given applied external voltage [20]. To this purpose we made use of the standard procedure of solution of linear networks based on Kirchhoff's laws. More precisely, in the present case of an irregular network with complex topology, it was particularly convenient to write and solve the Kirchhoff's node equations.

This one-node impedance model, henceforth also called AA model, is here further implemented by considering also the case of having two nodes for each amino acid, henceforth also called AB model. In fact, by identifying the amino acid with its C_α , in the one-node model

the resulting structure becomes analogous to the polypeptidic backbone. However, in this way only the backbone behavior can be reproduced while, in a conformational change, the backbone displacement is not the only relevant transformation. For example, one could be interested to study the rotations of each amino acid around the backbone [5]. To account for these possibilities, we have to depart from the one-node model, and look for a more realistic picture. Since the distinctive mark of each amino acid is in its residue, which does not lie on the polypeptidic backbone, we found natural to fix on each amino acid a second node. Accordingly, as second node we choose the so-called C_β atom, i.e. the second carbon atom that attaches to the functional group. The C_β atom is present in all the amino acids with the exclusion of glycine. The impedance attributed to the new links arising from the presence of this second node is taken of the same form as in Eq. (1). In this way, the total number of nodes (ν) mapping the protein is practically doubled. To connect the nodes we have adopted two choices, namely: The isotropic network and the directed network, this latter choice being able to better exploit directional characteristics in analogy with the directed percolation [21]. In the isotropic network, the α and β nodes are considered to be equivalent. Accordingly, each node is connected with all the others inside the interaction radius. Thus, for sufficiently large \mathbf{R} , each node has $\nu-1$ connections. In the directed network, the α and β nodes are not equivalent. Accordingly, for a given interaction radius, each α node, identified by the serial number of the protein primary structure, is connected to the β node of its amino acid and to the α and β nodes of amino acids with higher serial number. By contrast, each β node is linked to β nodes pertaining to amino acids with higher serial number.

Accordingly, for the isotropic network, the maximum value of the total number of links is:

$$N_{isotropic}^{max} = (N_\alpha + N_\beta)(N_\alpha + N_\beta - 1)/2, \quad (3)$$

while, for the directed network it is:

$$N_{directed}^{max} = (N_\alpha)(N_\alpha - 1)/2 + (N_\beta)(N_\beta - 1)/2 + \sum_{\alpha} \sum_{\beta \geq \alpha} N_\alpha N_\beta. \quad (4)$$

Here N_α is the number of C_α , coincident with the total number of amino acids, N , and N_β is the number of C_β . We observe that the considered proteins have, respectively, 348 C_α atoms and 325 C_β atoms (rhodopsin) and 527 C_α atoms and 483 C_β atoms (AChE), so we can assume $N_\beta \approx N$ and then deduce the expressions:

$$\begin{aligned} N_{isotropic}^{max} &\approx 2N(2N - 1)/2, \\ N_{directed}^{max} &\approx N(3N - 1)/2. \end{aligned} \quad (5)$$

By comparing Eqs. (3), (4), (5) we notice a global different functioning of the isotropic and directed networks. In the former network, each node represents an independent unity that interacts in the same way with all the other unities by elongating $(N_\alpha + N_\beta - 1) \approx 2N - 1$ links. In the latter network, each amino acid represents a working unit that interacts with other units through only three kinds of links, respectively: $C_\alpha - C_\alpha$, $C_\alpha - C_\beta$, and $C_\beta - C_\beta$. The number of links drawn out by each amino acid is $\approx 3N - 1$. We notice, that the isotropic network exhibits a number of links that is in general larger than the directed network up to a maximum value of about 25%.

In what concerns with the contacts to the external bias, in the AA model these are positioned on the first and last amino acid. In the AB model we have explored three possibilities. Accordingly, as injector and collector nodes we have taken: (i) the first C_α and

the last C_β , $AB_{\alpha,\beta}$ model; (ii) the couple $\alpha - \beta$ of the first amino acid, and the couple $\alpha - \beta$ of the last amino-acid, $AB_{\alpha\beta,\alpha\beta}$ model; (iii) the first C_α atom and the last C_α atom, $AB_{\alpha,\alpha}$ model.

III. RESULTS

In the following, we investigate the structural and electrical properties of a protein through both the graph model and the impedance network model. Then, we compare the electrical responses of a protein before and after undergoing a conformational change by using the AA and the AB models. The proteins under test are the bovine rhodopsin in dark (native) and light (activated), and the enzyme acetylcholinesterase (AChE) in the native form and complexed form with Huperzine A. The former is the most explored structure in the class of the GPCR and is widely used as a prototype for deducing the structure and function of all the other proteins pertaining to the same class [22, 23]. The latter plays a fundamental role in the process of functioning of the muscle cells. It destroys the neurotransmitter acetylcholine after it has passed to these cells the information coming from the brain, so that new signals can be transmitted. Starting from the atomic coordinates of the given protein, as reported in the public data base (PDB) [9], we first investigate the topological properties of the networks as function of the interaction radius. Then, the analogous investigation is carried out for the total impedance spectrum of the corresponding impedance network.

A. The topological network

Bovine rhodopsin and torpedo acetylcholinesterase are quite different proteins, both in structure and in functioning. The former is a seven- α -helices transmembrane protein, acting as a light receptor. It is able to capture photons, then producing a cascade process that starts with the activation of a G-protein and ends with the transmission of information to brain. The latter is a globular protein, made of fourteen β -sheets and sixteen α -helices. It is an enzyme that breaks the neurotransmitter acetylcholine into acetic acid and choline, thus stopping the transmission of signal from nerve cells to muscle cells.

At present, in the PDB [9] there are 26 entries related to bovine rhodopsin and 56 entries related to torpedo acetylcholinesterase. For rhodopsin, only two of the 26 entries describe the protein in light, namely: 1LN6, an NMR product, and the most recent 2I37, obtained with X-ray analysis. None of the above two entries reports the entire sequence of amino acids. For the rhodopsin in dark (the native state) there are three complete sequences, namely: 1U19, 2G87, 2HPY, all obtained by X-ray diffraction, with different resolution. The AChE is reported in many, incomplete, different representations, either native or complexed (the activated state) with different molecules (mainly Tacrine, Rivastigmine, Galantamine, Huperzine A/B).

The first task we address is to assess the level of resolution the present topological network model can reach when discriminates among similar (native or activated) representations and between the native and activated state. In other words, we would check whether the network provides a sensitive map of the protein structure. To this purpose, the analysis is performed by using the AA model.

Figure 1 reports the difference in the number of links between couples of structures of

rhodopsin, native (left) and activated (right), considered here as a function of the interaction radius. The native (Rho) and activated (MetaII) configurations refer to engineered structures obtained from the incomplete 1LN6, 1JFP and 1F88 (chain A) [15, 16, 17] and contain the same number of amino acids (348). The comparison among the three native representations of rhodopsin, 1U19, 2G87, 2HPY and the engineered one, Rho, shows that: (i) 1U19 and 2G87 exhibit practically the same number of links and, (ii) there are consistent differences between the native and engineered configurations. Furthermore, when moving from the native to the activated state, we found an increase of the difference in the number of links.

Figure 2 reports the difference in the number of links between couples of native (left) and complexed (right) representations of AChE as a function of the interaction radius. Here, the model correctly predicts that two distinct chains of the same representation of native AChE (1EA5_{a/b}) keep practically the same number of links independently of the interaction radius. On the other hand, representations of native AChE obtained under different experimental conditions show significative differences in the number of links, with a maximum value around $\mathbf{R} = 25 \text{ \AA}$. Some structures of complexed AChE are compared with the native form 2ACE: The difference in the link number can be positive or negative with respect to the structure considered, and the maxima differences are comparable with those between couples of native structures. By comparing rhodopsin with AChE, we notice that the values of the difference in the number of links and their dependence upon \mathbf{R} are very similar, either in the native or in the activated state. However, we remark that AChE with its 527 amino acids (2ACE) is a protein substantially greater than rhodopsin with its 328 amino acids. As a consequence, the relative value of the difference in the number of links is found to be more consistent for rhodopsin than for AChE.

From figures 1 and 2, it is also evident that the representations of a given protein in the same state (native or activated) look sometimes comparable with those of representations of the same protein in different states. In other words, different experimental conditions may produce very different representations of the same state of the protein. Therefore, if the network model is used to discriminate between the native and the activated (or complexed) state of the protein, then, it is mandatory that the reference representations should be produced under the same experimental conditions. For this reason, in the following we use the couple Rho - MetaII, for native and activated rhodopsin, and 2ACE - 1VOT-2 (X-ray products, same experiment) for native and complexed (with Huperzine A) AChE. The 1VOT-2 structure is the amino-acid sequence 1VOT deprived of two amino acids, ALA536, CYS537, which are not present in 2ACE.

To emphasize the network model ability to catch the protein topology, we have calculated the adjacency matrix [24] by representing the links in a x-y plane where the serial number of protein amino acids is reported on the x and y axes. Here each link corresponds to a point. Accordingly, Fig. 3 reports the map of rhodopsin in dark, Rho: The helix-to-helix links are very evident, either for $\mathbf{R} = 6 \text{ \AA}$ (dark points) or, even better, for $\mathbf{R} = 12 \text{ \AA}$ (grey boxes). We find that the links reproduce the closeness of H2 with H3 and H1, and of H2 and H4; furthermore they suggest the presence of H-bonds among H1, H2, H7 and H2, H3, H4 and also between H3 and H6 and between H6 and H7 [23]. Notice that the helix couples (H1-H3), (H1-H4), (H1-H5), (H1-H6), (H2-H5), (H2-H6), (H2-H6), (H4-H7), (H5-H7) are not connected for these values of the interaction radius.

Figure 4 reports the map of AChE. The adjacency matrix has been calculated for $\mathbf{R} = 6 \text{ \AA}$ (dark points), and for $\mathbf{R} = 12 \text{ \AA}$ (grey boxes). Here we notice an inhomogeneous

distribution of links, which is more tangled than in rhodopsin, mainly due to the higher complexity of the AChE protein. It is impossible, within a single figure, to report all the connections among sheets and helices. Thus, we emphasize only some of the them, the most evident, mainly reproducing the closeness between β -sheets.

We conclude that the graph analysis of proteins provides a valuable sketch of the force connected regions in the protein. In fact, by considering short range forces and using \mathbf{R} as the parameter describing their cut-off distance, Figs. 3 and 4 identify the interacting regions of the protein. The increase of \mathbf{R} is equivalent to consider forces with longer range. Accordingly, the drawings in Figs. 3 and 4 emphasize the dependence from the interacting radius of the connective map of the network.

B. The impedance network

By attributing to each link of the network an elementary impedance as given by Eq. (1), we have calculated the frequency response of the impedance network, $Z(f)$, in the frequency range 0÷1100 Hz, and represented it by means of the Nyquist plot. This kind of plot is very used in signal processing and in characterizing the electrical properties of biological materials appropriately deposited on functionalized gold electrodes [25]. It combines the imaginary and real part of a transfer function, in our case the impedance associated with the protein, using the frequency as an implicit variable. By means of the Nyquist plot, we compare the electrical response of the protein in its native and activated states for different values of the interaction radius.

The AA model contains one free parameter in the value of the cut-off radius \mathbf{R} , which fixes the number of links and so the network topology. In the limit of \mathbf{R} values too small (to say $\mathbf{R} < 6 \text{ \AA}$), only the nearest neighbours are connected, and so it is not possible to reveal the existence of more complex structure like α -helices or β -sheets. On the other hand, in the limit of \mathbf{R} values too large (to say $\mathbf{R} > 80 \text{ \AA}$), each node is connected with all the others, and so the protein appears as a uniform structure. A value of \mathbf{R} that is relevant for our purposes should be that which enables the main structures of the protein to emerge clearly. In fact, we are interested in detecting if and how they displace in the protein conformational change. Accordingly, we look for a value of \mathbf{R} best revealing the main structures of protein but also emphasizing the differences between the activated and the native state of the protein. For a GPCR, a relevant value of \mathbf{R} is a compromise between the characteristic dimension of the α -helices and the typical distance among α -helices, say D. When rhodopsin goes from the quiescent to the active state, its α -helices change their relative distance and D goes in D'. In the corresponding network, when the value of \mathbf{R} is between D and D', a huge number of links change their value, so well revealing the conformational change. We call D the "effective distance", and use it as a reference length value.

In order to explore the different topologies associated with the changing of \mathbf{R} , in the frame of the AA model, we have evaluated the network degree distribution, i.e. the distribution of the connected nodes [24]. The results of calculations are reported in Fig. 5 for rhodopsin and in Fig. 6 for AChE. Here we observe that for $\mathbf{R} \leq 9 \text{ \AA}$, both for rhodopsin and AChE, the degree distribution remains substantially peaked around the same degree value, i.e., there is a single characteristic dimension of the network clustering. It corresponds to the nearest neighboring domain (k=6 for AChE, k=7 for Rho). The cluster dimension grows for enlarged \mathbf{R} , until the value $\mathbf{R} = 12 \text{ \AA}$ for rhodopsin and $\mathbf{R} = 9 \text{ \AA}$ for AChE. We notice, indeed, that for $\mathbf{R} = 12 \text{ \AA}$ the degree distribution of rhodopsin exhibits two prominent maxima at k = 25

and 37, respectively (see Fig. 5), and so we have two different clusterizations. On the other hand, for the same value of \mathbf{R} , AChE exhibits a degree distribution randomly spiked in the range $20 < k < 45$. For values of \mathbf{R} in the range $12 \div 25 \text{ \AA}$, we have found a spreading of the distribution, which exhibits a series of spikes representing the fingerprint of the tertiary structure of the given protein. For values of $\mathbf{R} > 25 \text{ \AA}$, the degree distribution is found to shrink (see insert in Fig. 6) and, at $\mathbf{R} = 80 \text{ \AA}$, all the nodes are found to be practically connected each other. Here the degree distribution takes a delta-like shape centered at $k=(\nu-1)$. We conclude that, $\mathbf{R} = 9 \text{ \AA}$, for AChE, and $\mathbf{R} = 12 \text{ \AA}$, for rhodopsin, should be taken as optimal values to obtain the best resolution of the intimate protein structures.

From the above considerations, in the following we discuss four possible cases, in which the interaction radius \mathbf{R} , and the effective distance D combine to produce different resolutions for the AA and AB directed model, respectively. (Notice that the effective distance for the AB model has been assumed larger than that for the AA model because of the finite size of the amino acid.)

$$\begin{array}{llll}
I. & D_{AA} \approx R, & D_{AB} \gtrsim R, & D'_{AA} \gtrsim R, & D'_{AB} > R \\
II. & D_{AA} \lesssim R, & D_{AB} \approx R, & D'_{AA} \gtrsim R, & D'_{AB} \gtrsim R \\
III. & D_{AA} < R, & D_{AB} \lesssim R, & D'_{AA} \lesssim R, & D'_{AB} \gtrsim R \\
IV. & D_{AA} \ll R, & D_{AB} < R, & D'_{AA} \ll R, & D'_{AB} < R
\end{array} \tag{6}$$

Keeping in mind that the condition $D < R$ produces links and that, on the contrary, $D > R$ does not, the preceding cases are analyzed as follows:

Case I. Here the AA model discriminates different protein states better than the AB model.

Case II. Here both the AA and the AB models are able to resolve well the two configurations. In particular, the AA model is more sensitive to the change of the interaction radius.

Case III. Here the AA model discriminates different protein states worse than the AB model.

Case IV. Here it is rather difficult to discriminate the configurations both for the AA and the AB models since the number of links remains practically the same in both the configurations.

The general trends discussed above can be quantitatively assessed for the proteins under test by selecting a significative set of \mathbf{R} values for rhodopsin and AChE, respectively. Accordingly, for rhodopsin we take the \mathbf{R} values 6, 12, 25, 50 \AA , and for AChE the \mathbf{R} values 6, 9, 12, 25 \AA . The results of calculations are reported with an accuracy of three digits (see Appendix), which is considered appropriate for an experimental validation of the model.

Figures from 7 to 9 report the Nyquist plots of the global network impedance, normalized to the value at zero frequency, $Z(0)$, for the case of the engineered representations of rhodopsin in the native state, Rho, and in the activated state, Meta II. In all the figures the AA model is compared with the AB models by adopting the same convention for the symbols. In each figure the plots corresponding to increasing values of \mathbf{R} are indicated as (a), (b), (c), (d) in clockwise orientation.

As a general trend, the shape of the Nyquist spectra remains quite close to that of a semicircle, typical of a single RC parallel impedance, except for small but significant deviations from the semicircle when $\mathbf{R} = 6 \text{ \AA}$.

Figure 7 shows the different impedance responses obtained with the AA model (tiny continuous line for Rho and dotted line for MetaII) and with the $AB_{\alpha,\alpha}$ directed model (bold continuous line for Rho, and dashed line for Meta II).

Figure 8 shows the Nyquist plots for the AA model and the $AB_{\alpha\beta,\alpha\beta}$ directed model, respectively.

Figure 9 shows the Nyquist plot for the AA model and the AB isotropic model.

For $R = 6 \text{ \AA}$, in all the cases the AA model exhibits a resolution between different configurations better than the AB models. Thereby, the value $R = 6 \text{ \AA}$ pertains to case I: This value is a good choice but not the best.

The value of $R = 12 \text{ \AA}$ provides the largest difference between the activated configuration and the native one. Furthermore, we find that the $AB_{\alpha,\alpha}$ directed model (see Fig. 7), and the $AB_{\alpha\beta,\alpha\beta}$ directed model (see Fig. 8) increase the differences, respectively of 7%, and 5% with respect to the AA model. The value $R = 12 \text{ \AA}$ pertains to case II: The best value for the AA model, a very good value for the AB directed model.

For $R = 25 \text{ \AA}$, the difference between the configurations starts to decrease for both the models, even if the directed AB model still exhibits a resolution increment with respect to that of the AA model of 7%, and 3% for its versions, $AB_{\alpha,\alpha}$ and $AB_{\alpha\beta,\alpha\beta}$, respectively. The value $R = 25 \text{ \AA}$ pertains to case III: For the AB models, this value of R is still a relevant one.

Finally, for $R = 50 \text{ \AA}$, the directed AB model exhibits a resolution increment with respect to that of the AA model, of 3%, and 1% for its versions, $AB_{\alpha,\alpha}$ and $AB_{\alpha\beta,\alpha\beta}$, respectively. The ability to resolve is decreasing but it remains significant for both the models. Accordingly the value of $R = 50 \text{ \AA}$ is on the boundary between case III and case IV.

Figure 9 reports the comparison between the AA and the isotropic AB model. We can observe, that for $R > 6 \text{ \AA}$ the compared models give practically the same results, in other words, the AB isotropic model does not improve the AA model. This outcome says that the AB isotropic model does not give to the C_β an active role, unlike the AB directed model. With respect to the directed model it contains much more links, many of them slightly varying in the conformational change. This excess of (invariant) links hides the small differences between the native and active states. So, while the larger effects due to C_α displacements can emerge once again, the smaller improvements due to the C_β displacements cannot be appreciated.

By performing the same investigation for the case of AChE, we noticed that the differences between the native and activated configurations are significantly smaller than those of rhodopsin. In the AA model, with $R = 6 \text{ \AA}$ we have found a difference of only 6 %, while, for rhodopsin it was of 16 %. Furthermore, this difference decreases at increasing R , unlike the case of rhodopsin. This implies a low level of resolution between the configurations, even for the most sensitive AB directed model. Accordingly, in Figs. 10 and 11 we report only the comparison between the AA model and the directed $AB_{\alpha,\beta}$ model, which among the AB models exhibits the best resolution.

From Fig. 10, we observe that for $R = 6 \text{ \AA}$ the AA model shows a resolution higher than that of the AB model, as expected in case I. For $R = 9 \text{ \AA}$ the difference between the native and activated configuration is less than 0.1 % in the AA model and it is of 2 % in the directed AB model, as expected in case III. Figure 10 (c) emphasizes this difference.

Figure 11 reports the Nyquist plot of AChE for $R = 12 \text{ \AA}$ and 25 \AA , respectively. We notice that in both cases the AA model is no longer able to resolve the native from the activated configuration, while the directed AB model resolves a difference between the configurations of 2 % for $R = 12 \text{ \AA}$, as expected in case III. For $R = 25 \text{ \AA}$, also the directed AB model is no longer able to resolve the difference between the configurations, as expected in case IV.

In Figs. 7 to 10, it is shown that for $\mathbf{R} = 6 \text{ \AA}$, the Nyquist plots take shapes, which are slightly squeezed and asymmetric semicircles instead of the perfect semi-circle pertaining to a single RC parallel circuit (see Appendix for details). However, by increasing the value of \mathbf{R} , the Nyquist plots better and better approach the perfect semi-circle. The above peculiarities can be satisfactorily interpreted in terms of the Cole-Cole function [26] with one fitting parameter. Accordingly, to interpret the Nyquist plot, we use the normalized dimensionless response function [27]:

$$I_\omega \equiv (Z(\omega) - Z_\infty)/(Z(0) - Z_\infty) \quad (7)$$

which, in our case, reduces to $Z(\omega)/Z(0)$. The Cole-Cole fitting function is:

$$I_\omega = \frac{1}{1 + (i\omega\tau)^{1-\alpha}}, \quad 0 \leq \alpha \leq 1 \quad (8)$$

which leads to the following relation between the real and imaginary parts of I_ω

$$(\mathcal{R}(I_\omega) - \frac{a}{2})^2 + (\mathcal{I}(I_\omega) - \frac{b}{2})^2 = \frac{1}{c}(1 - a) + \frac{1}{4} \quad (9)$$

with

$$\begin{aligned} a &= \cos(\pi\alpha/2) \\ b &= \sin(\pi\alpha/2) \\ c &= 1 + (\omega\tau)^{2(1-\alpha)} + 2(\omega\tau)^{1-\alpha}b \end{aligned}$$

where $1/\tau = \omega_M$ is the frequency value corresponding to the maximum value taken by $-\mathcal{I}(I_\omega)$ as function of $\mathcal{R}(I_\omega)$ (see Appendix).

Figure 12 reports the fitting of the Nyquist plot for 2ACE, with $\mathbf{R} = 6 \text{ \AA}$ in the AA model, obtained with the Cole-Cole function [26] and $\alpha = 0.09$ together with the ideal semi-circle shape corresponding to $\alpha = 0$. The fact that for $\mathbf{R} > 6 \text{ \AA}$ the Nyquist plots take the ideal semi-circle shape is explained by the predominance increase of parallel with respect to serial connections. Thus, the network is no longer able to resolve the single relaxation times pertaining to each RC link but exhibits an average time constant.

The Cole-Cole function is one of the most used fitting functions in relaxation processes deviating from the Debye-Maxwell behavior [28]. It is not the unique, of course, due the complexity of the possible origins of this deviation [27, 29]. On the other hand, it has been shown that its meaning is more vast than simple fitting function [30]. In fact, while the power spectrum $|I_\omega|^2$ associated with the Debye-Maxwell function is Lorentzian, and the correlation function is exponential, the power spectrum associated with the Cole-Cole function is a more tangled object. It reduces to the Lorentzian distribution for $\alpha = 0$, furthermore, it goes like $(\omega\tau)^{-2(1-\alpha)}$ for $\omega\tau \gg 1$ and like $(1 + 2(\omega\tau)^{(1-\alpha)}\sin(\pi\alpha/2))^{-1}$ for $\omega\tau \ll 1$. The corresponding correlation function is the Mittag-Leffler function [31] which interpolates between a stretched exponential pattern ($\omega\tau \gg 1$) and an inverse power law decay ($\omega\tau \ll 1$). The exponent of both the functions is the same, $1-\alpha$.

For completeness, in the Appendix we report the single resistance and capacitance values corresponding to the calculated Nyquist plots.

IV. CONCLUSIONS

We have carried out a systematic analysis of protein modelling by means of a coarse grained network approach. As application we considered the case of bovine rhodopsin, the prototype of the GPCR family, and the case of AChE enzyme, whose inhibition is one of the most qualified treatments of the Alzheimer disease.

By using the topological features of the network, some relevant PDB entries have been compared in terms of the number of links as function of the interacting radius. We notice that the network map of the protein is able to distinguish among different PDB entries, and also to reproduce, with a fine choice of the cut-off \mathbf{R} , some topological properties of the protein structures. We conclude that the network approach is a suitable tool to discriminate among different protein structures.

By using the features of the impedance network associated with the topological one, we have investigated the dynamic electrical response of the proteins through the Nyquist plot representation. Accordingly, we predict for the rhodopsin an electrical response which is of a quite detectable level (up to difference of 22 % when passing from the native to the activated state). Furthermore, a significative conformational change is identified both with the one-node AA model and with the two-nodes AB models, the latter foreseeing significantly larger differences among the configurations. These results are supported by some experimental evidences [25]: Bovine rhodopsin and the rat olfactory receptor I7 has been immobilized on a gold electrode building up a self-assembled multilayer. The electrochemical characteristic of these structures has been performed in a standard electrochemical cell, and has shown Nyquist plots qualitatively similar to those obtained in the present paper.

Finally, we have found that the electrical responses of bovine rhodopsin and torpedo AChE are quite different, with regard to the possibility to distinguish between the activated and native state. For the couple 2ACE-1VOT-2, the maximal difference is of 6 %, and it is obtained for a small value of the interaction radius $\mathbf{R} = 6 \text{ \AA}$. We conclude that such a small sensitivity is due to an effectively small difference between the two states. Furthermore, since the maximal resolution between the native and the activated state is for small values of \mathbf{R} , the conformational change acts only among nearest neighboring. However, this is not the only possibility. In fact, in a recent work on a particular enzyme, the cyclophilin A (CypA) [32], it has been shown that also in the native form, the enzyme lives part in the activated and part in the native state. In the activated state, the percentage of activated configurations simply increases. According to this conclusion, also for AChE, our results should demonstrate that the crystallographic image of native AChE is a mix of the native state and of the Huperzine A (in our case) state, and therefore its conformational is of weak relevance.

V. ACKNOWLEDGMENTS

The authors acknowledge the MIUR PRIN "Strumentazione elettronica integrata per lo studio di variazioni conformazionali di proteine tramite misure elettriche" prot.2005091492. We thank also dr.V. Akimov for useful discussions on the subject and prof. M. Barteri for his interesting comments.

APPENDIX

The frequency response of the impedance network presented here can be modeled to a good degree of approximation, by the impedance of a single RC parallel circuit

$$Z_{RC} = \frac{R}{1 + i\omega RC} \equiv \mathcal{R} + i\mathcal{I}, \quad (\text{A.1})$$

where \mathcal{R}, \mathcal{I} indicates the real and imaginary part of Z_{RC} , respectively. It is convenient to normalize the impedance, in order to better compare results coming from different proteins and boundary conditions, so we introduce

$$\hat{Z}_{RC} = \frac{Z_{RC}}{R} \equiv \hat{\mathcal{R}} + i\hat{\mathcal{I}}, \quad (\text{A.2})$$

with R the impedance at zero frequency. Notice that the function (A.2) is a first order function, i.e. it has only one pole in frequency and it is stable. The maximum of $-\hat{\mathcal{I}}$ occurs for $-\hat{\mathcal{I}} = \hat{\mathcal{R}} = 1/2$ and is obtained for $\omega = \omega_M = 1/RC$.

In the Nyquist plots calculated for the impedance networks, to account for the non-ideal semicircle shape, we have determined the frequency ω^* at which $-\hat{\mathcal{I}} = \hat{\mathcal{R}}$ and defined an effective capacitance, C^* , by the relation $\omega^* = 1/RC^*$. The difference between the values of C and C^* is a signature of the deviation of the Nyquist plot from the perfect semi-circle shape. The values of R , C , and C^* corresponding to the Nyquist plots reported in Figs. 7, 8, 10, 11 are reported in Table I (rhodopsin) and in Table II (AChE).

-
- [1] C. C. Moser, J. M. Keske, K. Warncke, R. S. Farid, and P. L. Dutton, *Nature* **355**, 796 (1992) and references therein.
 - [2] T. Fisher Weiss, *Cellular Biophysics*, Vol. 2, 2th ed. (The MIT Press, Cambridge, Massachusetts, 1997).
 - [3] H. Fraufelder, P. G. Wolynes, and R. H. Austin, *Rev. Mod. Phys.* **71**, S419 (1999).
 - [4] J. N. Onuchic, D. N. Beratan, J. R. Winkler, and H. B. Gray, *Annu. Rev. Biophys. Biomol. Struct.* **21**, 349 (1992); V. S. Pande, and J. N. Onuchic, *Phys. Rev. Lett.* **78**, 146 (1997).
 - [5] S.-Y. Sheu, D.-Y. Yang, H. L. Selzle, and E. W. Schlag, *Eur. Phys. J. D* **20**, 557 (2002); E. W. Schlag, S.-Y. Sheu, D.-Y. Yang, H. L. Selzle, and S. H. Lin, *J. Phys. Chem.* **104**, 7790 (2000).
 - [6] R. Rinaldi, A. Biasco, G. Maruccio, R. Cingolani, D. Alliata, L. Andolfi, P. Facci, F. De Rienzo, R. Di Felice, E. Molinari, M. Verbeet, and G. Canters, *Appl. Phys. Lett.* **82**, 472 (2003).
 - [7] Y. Jin, N. Friedman, M. Sheves, T. He, and D. Cahen, *PNAS* **103**, 8601 (2006).
 - [8] T. V. Dinh, B. M. Cullum, and D. L. Stokes, *Sens. Act. B* **74**, 2 (2001).
 - [9] H. M. Berman, J. Westbrook, Z. Feng, G. Gilliland, T. N. Bhat, H. Weissing, I. N. Shindyalov, and P. E. Bourne, *Nucleic Acids Research* **28**, 235 (2000).
 - [10] A. McCammon, and S. C. Harvey, *Dynamics of Proteins and Nucleic Acids* (Cambridge University Press, 1987); A. Kitao, and N. Go, *Curr. Opin. Struct. Bio.* **9**, 164 (1999); P. Carloni, U. Rothlisberger, and M. Parrinello, *Acc. Chem. Res.* **35**, 455 (2002).

- [11] D. ben-Avraham, Phys. Rev. B **47**, 14559 (1993); C. Micheletti, G. Lattanzi, and A. Maritan, J. Mol. Biol. **321**, 909 (2002).
- [12] M. Tirion, Phys. Rev. Lett. **77**, 1905 (1996).
- [13] A. R. Atilgan, S. R. Durell, R. L. Jernigan, M. C. Demirel, O. Keskin, and I. Bahar, Biophys. J. **80**, 505 (2001); M. K. Kim, R. L. Jernigan, and G. S. Chirikjian, Biophys. J. **89**, 43 (2005).
- [14] C. Micheletti, G. Lattanzi, and A. Maritan, J. Mol. Biol. **321**, 909 (2002); C. Micheletti, P. Carloni, and A. Maritan, Proteins **55**, 635 (2004).
- [15] E. Alfinito, V. Akimov, C. Pennetta, and L. Reggiani, in *Unsolved Problems of Noise and Fluctuations, AIP Conference Proceedings 800*, edited by L. Reggiani, C. Pennetta, V. Akimov, E. Alfinito, and M. Rosini (AIP, Melville, New York, 2005), pp.381-387.
- [16] C. Pennetta, V. Akimov, E. Alfinito, L. Reggiani, T. Gorojankina, J. Minic, E. Pajot-Augy, M. A. Persuy, et al, in *Nanotechnologies of the Life Science,4* edited by Challa S. S. R. Kumar (Wiley-VCH, Weinheim, 2006), pp. 217-240.
- [17] C. Pennetta, V. Akimov, E. Alfinito, L. Reggiani, and G. Gomila, in *Noise and Information in Nanoelectronics, Sensors and Standards II- Proceedings of SPIE 5472*, edited by J. M. Smulko, Y. Blanter, M. I. Dykman, and L. B. Kish (Int. Soc. Opt. Eng. Bellingham, 2004) pp. 172-182.
- [18] H. Yang, G. Luo, P. Karnchanaphanurach, T. M. Louie, I. Rech, S. Cova, L. Xun, and X. S. Xie, *Sciences* **302**, 262 (2003).
- [19] X. Song, J. Chem. Phys. **116**, 9359 (2002).
- [20] R. Rammal, C. Tannous, and A. M. S. Tremblay, Phys. Rev. A **31**, 2662 (1985).
- [21] G. Ódor, Rev. Mod. Phys. **76**, 663 (2004) and references therein.
- [22] U. Gether, and B. K. Kobilka, J. Bio. Chem. **273**, 17979 (1998); R. J. Lefkowitz, Nature Cell Biology **2**, E133 (2000); K. Palczewski, T. Hori, C. A. Behnke, H. Motoshima, B. A. Fox, I. Le Trong, D. C. Teller, T. Okada, R. E. Stenkamp, M. Yamamoto, and M. Miyano, Science **289**, 739 (2000).
- [23] S. T. Menon, M. Han, and T. P. Sakmar, Physio. Rev. **81**, 1659 (2001).
- [24] R. Albert, and A. L. Barabasi, Rev. Mod. Phys. **74**, 47 (2002).
- [25] Y. Hou, N. Jaffrezic-Renault, C. Martelet, A. Zhang, J. Minic-Vidic, T. Gorojankina, M-A. Persuy, E. Pajot-Augy, et al., Biosensors and Bioelectronics **21**, 1393 (2006); Y. Hou, S. Helali, A. Zhang, N. Jaffrezic-Renault, C. Martelet, J. Minic, T. Gorojankina, M-A. Persuy, et al. Biosensors and Bioelectronics **22**, 1550 (2007).
- [26] K. S. Cole, and R. H. Cole, J. Chem. Phys. **9**, 341 (1941).
- [27] J. R. Macdonald, J. Appl. Phys. **62**, R51 (1987) and references therein.
- [28] P. Debye, *Polar Molecules* (The Chemical Catalogue Company, New York, 1929).
- [29] D. W. Davidson, and R. H. Cole, J. Chem. Phys. **19**, 1417 (1951); A. K. Jonscher, Nature **267**, 673 (1977); K. L. Ngai, Phys. Rev. B **22**, 2066 (1980); V. Raicu, Phys. Rev. B **60**, 4677 (1999).
- [30] R. Metzler, and J. Klafter, J. Non-Crystal. Sol. **305**, 81 (2002); K. Weron, and M. Kotulski, Physica A **232**, 180 (1996).
- [31] A. Erdélyi (Ed.), *Tables of Integral Transformations* Bateman Manuscript Project, Vol.1 (McGraw-Hill, New York, 1954)
- [32] E. Z. Eisenmesser, O. Millet, W. Labeikovsky, D. M. Korzhnev, M. Wolf-Wartz, D. A. Bosco, J. J. Skalicky, L. E. Kay, and D. Kern, Nature Lett. **483**, 117 (2005).

TABLE I: Resistance and capacitances of the RC single-impedance circuit equivalent to the protein impedance network. Model AA is compared with the $AB_{\alpha,\beta}$ and $AB_{\alpha\beta,\alpha\beta}$ models for $R=6,12,25,50$ Å. Rhodopsin is the analyzed protein

	AA Model			$AB_{\alpha,\alpha}$ Model			$AB_{\alpha\beta,\alpha\beta}$ Model		
R /Type	R ($P\Omega$)	C(fF)	C*(fF)	R($P\Omega$)	C(fF)	C* (fF)	R($P\Omega$)	C(fF)	C*(fF)
$R=6\text{\AA}$									
Rho	$9.49 \cdot 10^3$	$1.53 \cdot 10^{-4}$	$1.32 \cdot 10^{-4}$	$4.72 \cdot 10^3$	$3.26 \cdot 10^{-4}$	$2.82 \cdot 10^{-4}$	$4.47 \cdot 10^3$	$3.60 \cdot 10^{-4}$	$3.19 \cdot 10^{-4}$
Meta	$1.13 \cdot 10^4$	$1.21 \cdot 10^{-4}$	$9.31 \cdot 10^{-5}$	$5.37 \cdot 10^3$	$2.66 \cdot 10^{-4}$	$1.86 \cdot 10^{-4}$	$5.01 \cdot 10^3$	$3.07 \cdot 10^{-4}$	$2.50 \cdot 10^{-4}$
$R=12\text{\AA}$									
Rho	$2.51 \cdot 10^2$	$5.37 \cdot 10^{-3}$	$5.16 \cdot 10^{-3}$	$1.29 \cdot 10^2$	$9.69 \cdot 10^{-3}$	$9.69 \cdot 10^{-3}$	$9.07 \cdot 10^1$	$1.47 \cdot 10^{-2}$	$1.43 \cdot 10^{-2}$
Meta	$3.22 \cdot 10^2$	$3.57 \cdot 10^{-3}$	$3.41 \cdot 10^{-3}$	$1.81 \cdot 10^2$	$5.51 \cdot 10^{-3}$	$5.01 \cdot 10^{-3}$	$1.24 \cdot 10^2$	$9.35 \cdot 10^{-3}$	$8.93 \cdot 10^{-3}$
$R=25\text{\AA}$									
Rho	$1.67 \cdot 10^1$	$6.90 \cdot 10^{-2}$	$6.90 \cdot 10^{-2}$	$1.07 \cdot 10^6$	$1.04 \cdot 10^{-1}$	$9.82 \cdot 10^{-2}$	5.99	$1.99 \cdot 10^{-1}$	$1.96 \cdot 10^{-1}$
Meta	$2.04 \cdot 10^1$	$5.38 \cdot 10^{-2}$	$5.38 \cdot 10^{-2}$	$1.42 \cdot 10^6$	$7.04 \cdot 10^{-2}$	$7.04 \cdot 10^{-2}$	7.06	$2.83 \cdot 10^{-1}$	$2.83 \cdot 10^{-1}$
$R=50\text{\AA}$									
Rho	2.31	$4.32 \cdot 10^{-1}$	$4.32 \cdot 10^{-1}$	1.61	$5.65 \cdot 10^{-1}$	$5.65 \cdot 10^{-1}$	0.82	1.21	1.21
Meta	2.72	$3.34 \cdot 10^{-1}$	$3.34 \cdot 10^{-1}$	1.97	$4.24 \cdot 10^{-1}$	$4.24 \cdot 10^{-1}$	0.98	$9.30 \cdot 10^{-1}$	$9.30 \cdot 10^{-1}$

TABLE II: Resistance and capacitances of the RC single-impedance circuit equivalent to the protein impedance network. Model AA is compared with the $AB_{\alpha,\alpha}$ and $AB_{\alpha\beta,\alpha\beta}$ models, for $R = 6, 9, 12, 25$ Å. AChE is the analyzed protein

	AA Model			$AB_{\alpha,\beta}$ Model		
R /Type	$R(P\Omega)$	$C(\text{fF})$	$C^*(\text{fF})$	$R(P\Omega)$	$C(\text{fF})$	$C^*(\text{fF})$
$R = 6\text{\AA}$						
2ACE	$1.51 \cdot 10^4$	$7.23 \cdot 10^{-5}$	$6.00 \cdot 10^{-5}$	$3.63 \cdot 10^3$	$3.93 \cdot 10^{-4}$	$3.67 \cdot 10^{-4}$
1VOT-2	$1.43 \cdot 10^4$	$8.74 \cdot 10^{-5}$	$6.99 \cdot 10^{-5}$	$3.50 \cdot 10^3$	$4.08 \cdot 10^{-4}$	$3.57 \cdot 10^{-4}$
$R = 9\text{\AA}$						
2ACE	$1.45 \cdot 10^3$	$1.11 \cdot 10^{-3}$	$1.01 \cdot 10^{-3}$	$5.76 \cdot 10^2$	$2.89 \cdot 10^{-3}$	$2.67 \cdot 10^{-3}$
1VOT-2	$1.46 \cdot 10^3$	$1.10 \cdot 10^{-3}$	$1.07 \cdot 10^{-3}$	$5.88 \cdot 10^2$	$2.84 \cdot 10^{-3}$	$2.62 \cdot 10^{-3}$
$R = 12\text{\AA}$						
2ACE	$3.57 \cdot 10^2$	$5.10 \cdot 10^{-3}$	$5.10 \cdot 10^{-3}$	$1.42 \cdot 10^2$	$1.28 \cdot 10^{-2}$	$1.28 \cdot 10^{-2}$
1VOT-2	$3.57 \cdot 10^2$	$5.10 \cdot 10^{-3}$	$5.10 \cdot 10^{-3}$	$1.45 \cdot 10^2$	$2.51 \cdot 10^{-2}$	$2.51 \cdot 10^{-2}$
$R = 25\text{\AA}$						
2ACE	$2.08 \cdot 10^1$	$9.80 \cdot 10^{-2}$	$9.80 \cdot 10^{-2}$	9.71	$2.07 \cdot 10^{-1}$	$2.06 \cdot 10^{-1}$
1VOT-2	$2.08 \cdot 10^1$	$9.63 \cdot 10^{-2}$	$9.63 \cdot 10^{-2}$	9.76	$2.05 \cdot 10^{-1}$	$2.05 \cdot 10^{-1}$

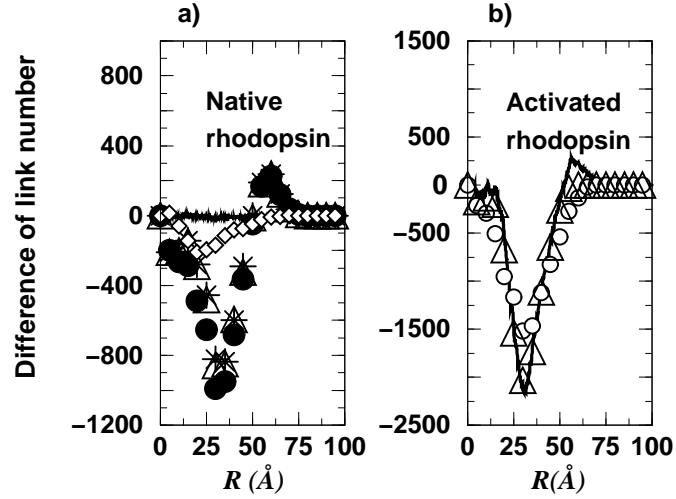


FIG. 1: Link number difference (LND) for different configurations of rhodopsin versus the interaction radius. All the configurations contain the same number of amino acids. Figure 1 (a): Native rhodopsin. Stars refer to the LND between the a-chain of 1U19, 1U19a and the engineered representation of native rhodopsin, Rho. Open triangles refer to the LND between the a-chain of 2G87, 2G87a and Rho. Full circles refer to the LND between the a-chain of 2HPY, 2HPYa and Rho. Open diamonds refer to the LND between the a-chains 2HPYa and 1U19a. Continuous line refers to the LND between 2G87a and 1U19a. Figure 1(b): Activated rhodopsin. Continuous line refers to the LND between the engineered representation of rhodopsin in light, MetaII, and Rho. Open circles refer to the LND between 2I37 and Rho. Open triangles refer to the difference between 1LN6 and Rho. In the second and third case the Rho sequence has been deprived of the amino acids that are not present in 2I37 and 1LN6, respectively.

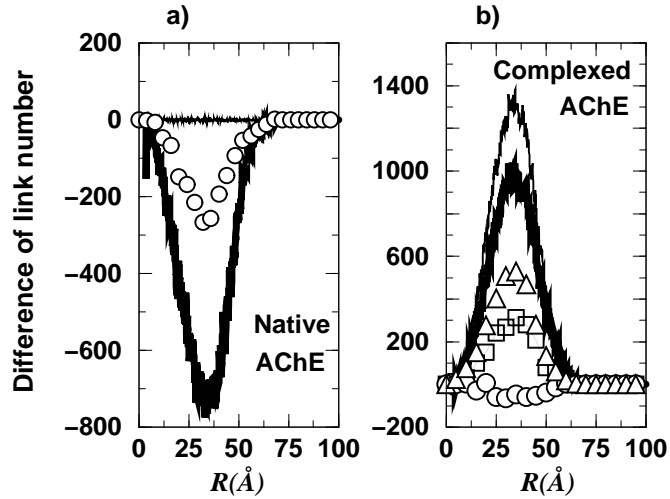


FIG. 2: Link number difference (LND) for different configurations of AChE versus the interaction radius. All the configurations contain the same number amino acids. Figure 2(a): Native configurations. Tiny continuous line refers to the LND between two chains of the 1EA5 representation: 1EA5*b*, 1EA5*a*. Bold continuous line refers to the difference between 1W75*a* and 2ACE. Open circles refer to both: the LND between 1EA5*a* and 1W75*b* and the LND between 1EA5*b* and 1W75*b*. Figure 2(b): Complexed configurations. Tiny black line refers to the LND between 2ACE and 1ACJ. Bold black line refers to the LND between 2ACE and 1ACL. Open squares refer to the LND between 2ACE and 1AX9. Open circles refer to the LND between 2ACE and 1VOT. Open triangles refer to the LND between 2ACE and 1GPK*a*.

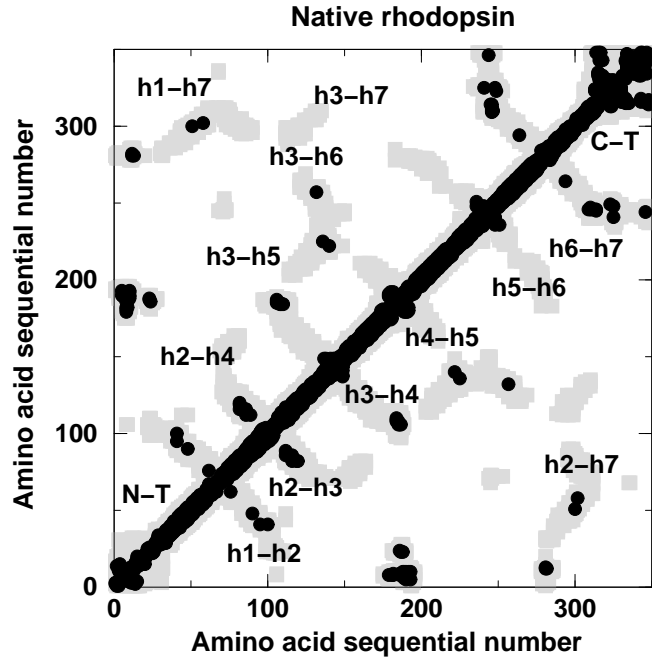


FIG. 3: Adjacency matrix of native rhodopsin, Rho. The x,y axes report the sequential number of the amino acids. Black full circles refer to $R = 6 \text{ \AA}$, and grey open squares to $R = 12 \text{ \AA}$. Each circle/square correspond to a link between the couple of amino acids (x,y). The main domains associated with the connections among closest helices are explicitly indicated.

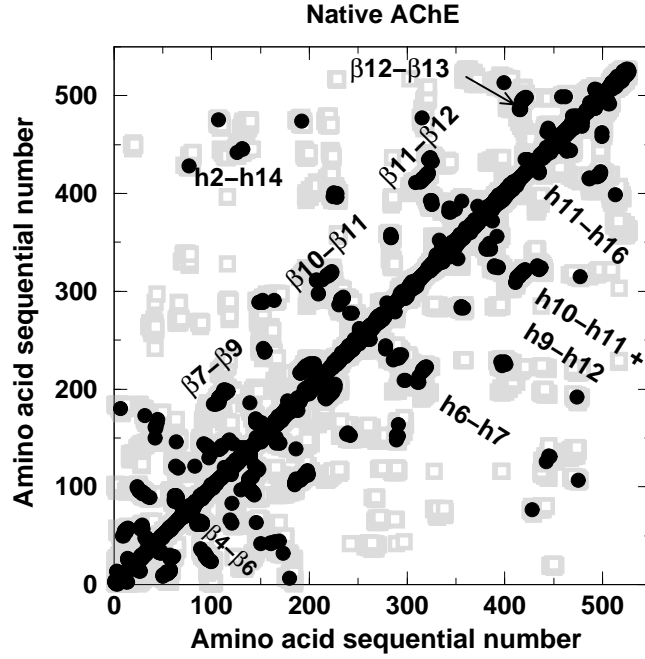


FIG. 4: Adjacency matrix of 2ACE. The x,y axes report the sequential number of the amino acid. Black full circles refer to $R = 6 \text{ \AA}$, and grey open squares to $R = 12 \text{ \AA}$. Each circle/square corresponds to a link between the couple of amino acids (x,y). Dashed lines are in correspondence with the three amino acids of the active site.

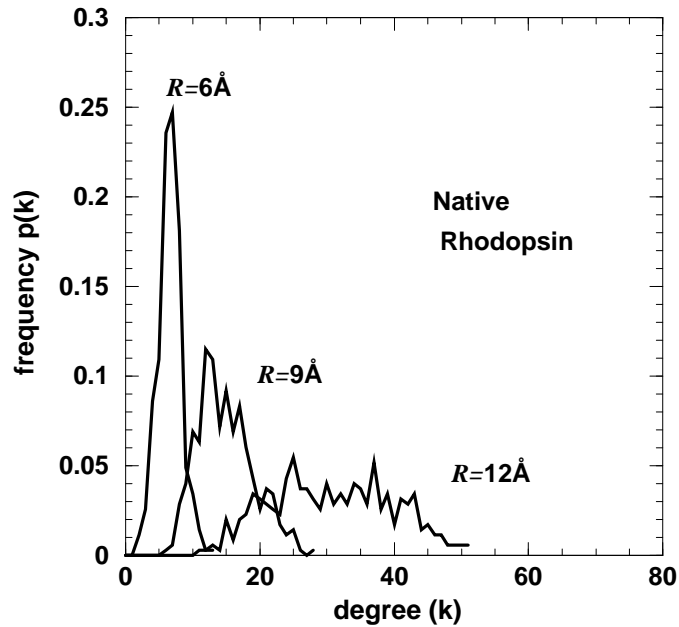


FIG. 5: Degree distribution of native-rhodopsin (rho) network for increasing values of the interaction radius R .

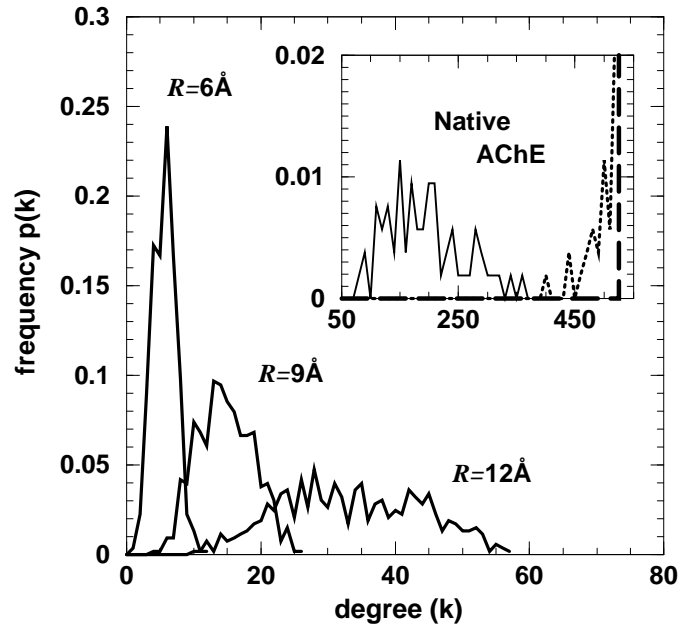


FIG. 6: Degree distribution of the native-AChE network for increasing values of the interaction radius R . The inset reports the degree distribution for $R = 25\text{\AA}$ (solid line), $R = 50\text{\AA}$ (dotted line), $R = 80\text{\AA}$ (bold dashed line).

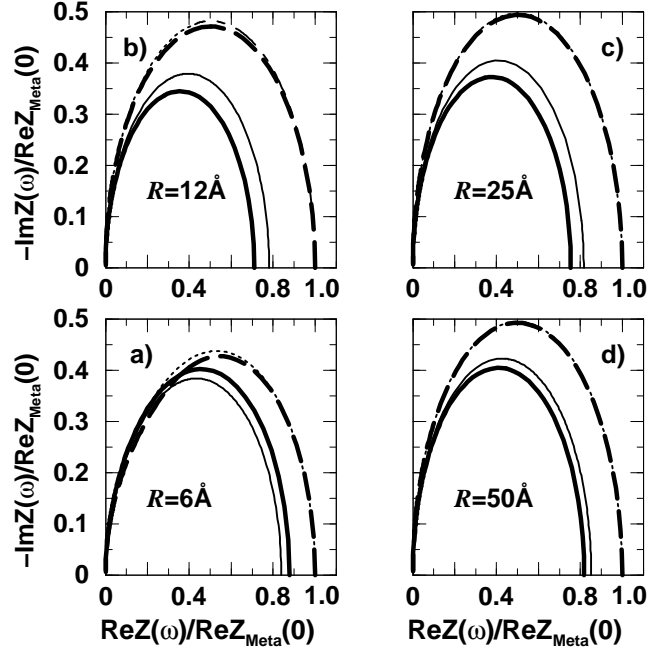


FIG. 7: Nyquist plots of the network impedance associated with the protein. Native rhodopsin is compared with activated rhodopsin. The protein sequences are the engineered Rho (native) and Meta II (activated). For the AA model: Continuous tiny lines refer to Rho, dotted lines refer to Meta II. For the $AB_{\alpha,\alpha}$ directed model: Bold continuous lines refer to Rho, dashed lines refer to Meta II. Plots are reported for increasing values of the interaction radius in the range from 6 Å to 50 Å following a clock-wise orientation.

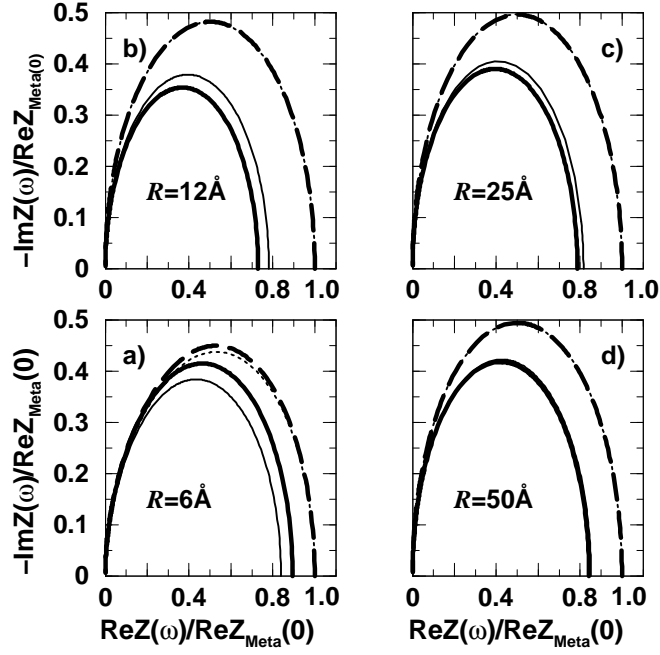


FIG. 8: Nyquist plot of the network impedance associated with the protein. Native rhodopsin is compared with activated rhodopsin. The protein sequences are the engineered Rho (native) and Meta II (activated). For the AA Model: Continuous tiny lines refer to Rho, and dotted lines refer to Meta II. For the $AB_{\alpha\beta, \alpha\beta}$ directed model: Bold continuous lines refer to Rho, and dashed lines refer to Meta II. Plots are reported for increasing values of the interaction radius in the range from 6 \AA to 50 \AA following a clock-wise orientation.

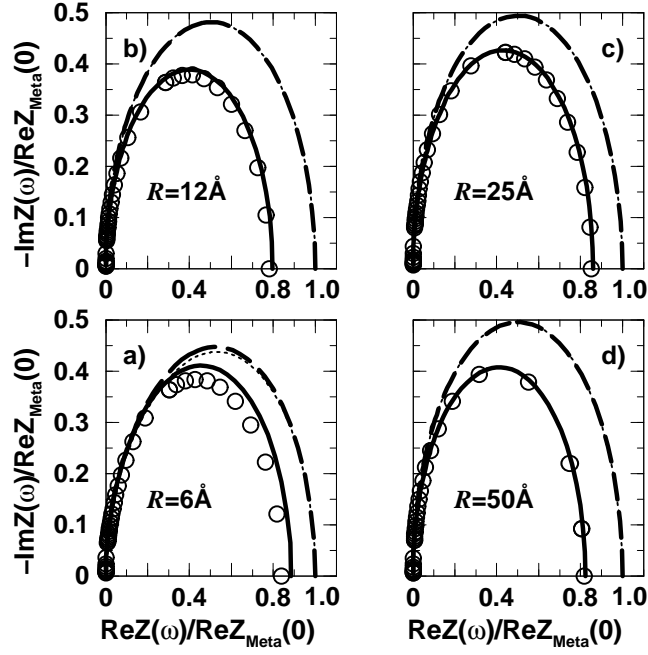


FIG. 9: Nyquist plot of the network impedance associated with the protein. Native rhodopsin is compared with activated rhodopsin. The protein sequences are the engineered Rho (native) and Meta II (activated). For the AA Model: Circles refer to Rho, and dotted lines refer to Meta II. For the AB isotropic model (with in-contact on the first C_α carbon atom and out-contact on the last C_α carbon atom): Bold continuous lines refer to Rho, and dashed lines refer to Meta II. Plots are reported for increasing values of the interaction radius in the range from 6\AA to 50\AA following a clock-wise orientation.

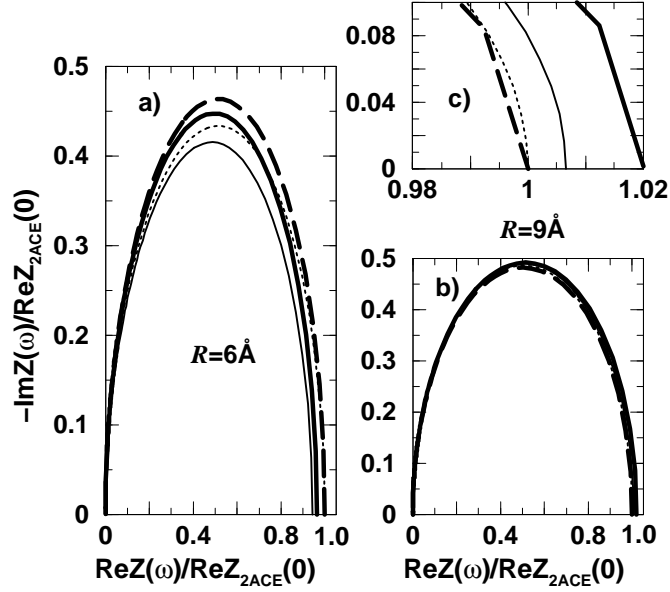


FIG. 10: Nyquist plot of the network impedance associated with the protein. Native AChE, 2ACE, is compared with AChE complexed with Huperzyne A, 1VOT-2. For the AA model: Tiny continuous lines refer to 1VOT-2, dotted lines refer to 2ACE. For the $AB_{\alpha,\beta}$ directed model: Bold continuous lines refer to 1VOT-2, and dashed lines refer to 2ACE in the directed $AB_{\alpha,\beta}$ model. In Fig. 9(a) $R = 6 \text{ \AA}$, while in Figs. 9(b) and 9(c) $R = 9 \text{ \AA}$; Fig. 9(c) is a zoom of Fig. 9(b).

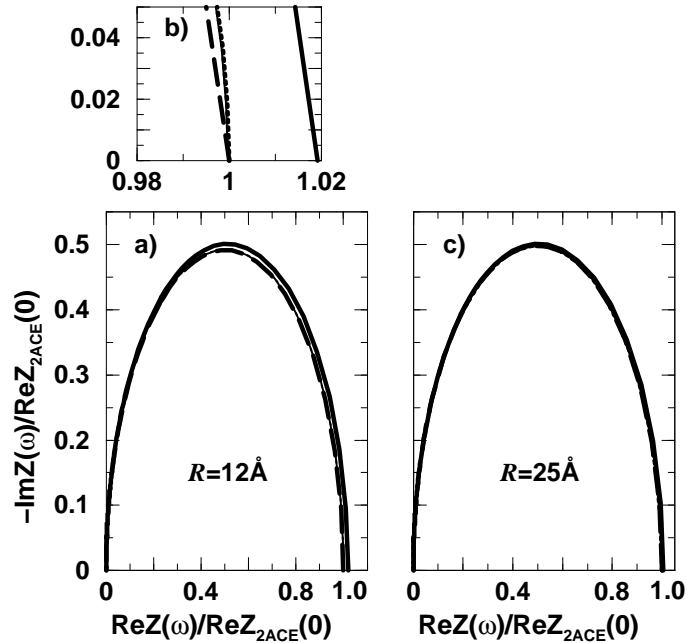


FIG. 11: Nyquist plot of the network impedance associated with the protein. Native AChE, 2ACE, is compared with AChE complexed with Huperzyne A, 1VOT-2. For the AA model: Tiny continuous lines refer to 1VOT-2, dotted lines refer to 2ACE. For the $AB_{\alpha,\beta}$ directed model: Bold continuous lines refer to 1VOT-2, and dashed lines refer to 2ACE in the directed $AB_{\alpha,\beta}$ model. In Figs. 10(a) and 10(b) $R = 12 \text{ \AA}$, and Fig. 10(b) is a zoom of Fig. 10(a). In Fig. 10(c) $R = 25 \text{ \AA}$.

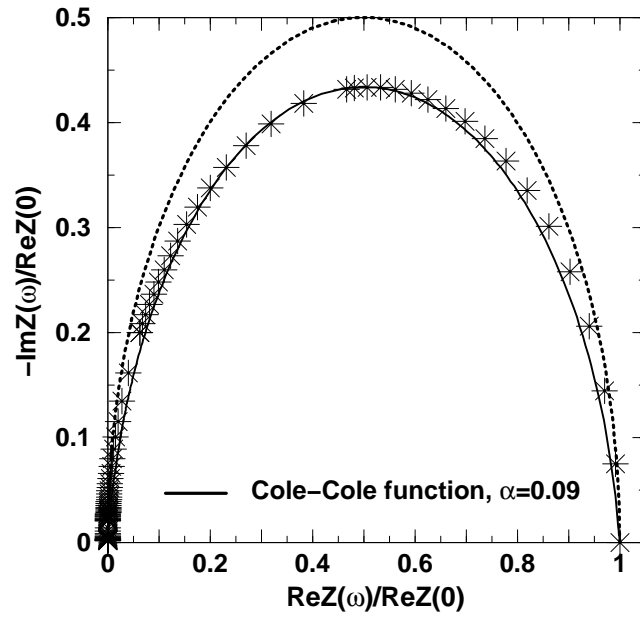


FIG. 12: Nyquist plot of the 2ACE for $R = 6 \text{ \AA}$, with the Cole-Cole distribution. Stars refer to data from simulations, the dotted line refers to the Debye distribution function, the continuous line refers to the Cole-Cole distribution function with the best fit parameter $\alpha = 0.09$. For all the distributions the value $\tau = 1.12 \text{ s}$ is used.